Biomaterials Science

ROYAL SOCIETY OF CHEMISTRY

PAPER

View Article Online
View Journal | View Issue

Cite this: *Biomater. Sci.*, 2022, **10**, 2940

In vivo delivery of plasmid DNA by lipid nanoparticles: the influence of ionizable cationic lipids on organ-selective gene expression†

Azizah Algarni, Emily H. Pilkington, Estelle J. A. Suys, Hareth Al-Wassiti, Colin W. Pouton* and Nghia P. Truong *

Ionizable cationic lipids play a critical role in developing new gene therapies for various biomedical applications, including COVID-19 vaccines. However, it remains unclear whether the formulation of lipid nanoparticles (LNPs) using DLin-MC3-DMA, an optimized ionizable lipid clinically used for small interfering RNA (siRNA) therapy, also facilitates high liver-selective transfection of other gene therapies such as plasmid DNA (pDNA). Here we report the first investigation into pDNA transfection efficiency in different mouse organs after intramuscular and intravenous administration of lipid nanoparticles (LNPs) where DLin-MC3-DMA, DLin-KC2-DMA or DODAP are used as the ionizable cationic lipid component of the LNP. We discovered that these three benchmark lipids previously developed for siRNA delivery followed an unexpected characteristic rank order in gene expression efficiency when utilized for pDNA. In particular, DLin-KC2-DMA facilitated higher *in vivo* pDNA transfection than DLin-MC3-DMA and DODAP, possibly due to its head group pK_a and lipid tail structure. Interestingly, LNPs formulated with either DLin-KC2-DMA or DLin-MC3-DMA exhibited significantly higher *in vivo* protein production in the spleen than in the liver. This work sheds light on the importance of the choice of ionizable cationic lipid and nucleic acid cargo for organ-selective gene expression. The study also provides a new design principle towards the formulation of more effective LNPs for biomedical applications of pDNA, such as gene editing, vaccines and immunotherapies.

Received 1st February 2022,
Accepted 20th April 2022

DOI: 10.1039/d2bm00168c

rsc.li/biomaterials-science

1. Introduction

The development of lipid nanoparticles (LNPs) has recently opened a new frontier for *in vivo* gene delivery and enabled several new gene therapies for use in humans.[1–3] In 2018, Onpattro became the first FDA-approved small interfering RNA (siRNA) LNP therapy to treat a peripheral nerve disease (*i.e.*, hereditary ATTR amyloidosis).[4] In 2020, two messenger RNA (mRNA) LNP vaccines were authorised for emergency use to prevent disease caused by SARS-CoV-2 infection (COVID-19).[5,6] Both siRNA and mRNA are susceptible to degradation and unable to cross cell membranes due to their negative charge.[7–10] Therefore, LNPs are key to the successful development of both Onpattro and COVID-19 mRNA vaccines.[11] LNPs encapsulate nucleic acids inside the core, protect them from degradation, carry them to a target organ, facilitate cellular uptake, trigger endosomal escape, and finally release them into the cell cytosol where they are activated.[11] To achieve high efficiency in delivering these genetic materials, LNPs are typically formulated from four components with different functions: an ionizable cationic lipid, a helper lipid, cholesterol, and a PEGylated lipid.[6]

Among the components of LNPs, the ionizable cationic lipid is crucial for achieving high *in vivo* gene transfection efficiency and played a decisive role in the development of Onpattro, the first FDA-approved gene therapy.[4] Although siRNA has received considerable interest and billion-dollar investments since the 2006 Nobel prize in medicine, its first translation to the bedside was realized twelve years later.[12] The long journey of ionizable cationic lipid development started from pioneering work by Michael Hope and coworkers demonstrating the first use of an ionizable cationic lipid, 1,2-dioleoyl-3-dimethylammoniumpropane (DODAP), to encapsulate nucleic acids inside LNPs.[13] Subsequently, MacLachlan *et al.* reported the use of a member of an analogous series of ionizable cationic lipids, 1,2-dilinoleyloxy-3-dimethylaminopropane (DLinDMA). DLinDMA with a similar head group to DODAP, but with two double bonds per alkyl chain instead of one,

Department of Drug Delivery, Disposition and Dynamics, Monash Institute of Pharmaceutical Sciences, Monash University, Melbourne, VIC 3052, Australia. E-mail: nghia.truong@monash.edu, colin.pouton@monash.edu

† Electronic supplementary information (ESI) available. See DOI: https://doi.org/10.1039/d2bm00168c

could significantly improve gene transfection efficiency.[14] Later, the Hope group further optimized the DLinDMA series and discovered that 2,2-dilinoleyl-4-(2-dimethylaminoethyl)-[1,3]-dioxolane (DLin-KC2-DMA) exceeded the gene silencing capacity of other DLinDMA lipids by a factor of ten.[15] The discovery of DLin-KC2-DMA was considered the first breakthrough in improving the potency and tolerability of siRNA LNP therapy for clinical use.[4] Two years later, a comprehensive investigation into the headgroup of more than 300 ionizable lipids led to the identification of dilinoleylmethyl-4-dimethylaminobutyrate (DLin-MC3-DMA), which exhibited improved siRNA knockdown efficiency: more than two orders of magnitude compared to the previous benchmark DLin-KC2-DMA formulation.[16] To date, DLin-MC3-DMA is still one of the best performing ionizable cationic lipids for liver-selective siRNA delivery and remains the main component in the Onpattro lipid formulation.[4]

While the role of DLin-MC3-DMA in the success of siRNA therapy is clear, it remains unknown whether this ionizable cationic lipid also facilitates high liver-specific transfection of other gene therapies such as plasmid DNA (pDNA). Unlike short siRNA (typically containing 20 to 27 base pairs), pDNA sequences are orders of magnitude longer (from 1000 base pairs to over 100 000 base pairs).[17] In addition, pDNA is transcribed into new mRNA molecules in the cell nucleus while siRNA acts within the cell cytosol to degrade endogenous mRNA.[18,19] Such distinct differences in the delivery requirements of siRNA and pDNA suggest that LNPs and ionizable cationic lipids optimized for the efficient delivery of pDNA may be quite different to those optimized for siRNA. Identification of suitable ionizable cationic lipids for achieving high *in vivo* pDNA transfection efficiency is highly desirable as pDNA has diverse applications ranging from research tools to therapies.[20] For instance, pDNA can be used in laboratories for genome editing,[21] or to exploit cells to produce proteins such as monoclonal or bispecific antibodies.[21] With sufficiently high *in vivo* transfection efficiency, pDNA can also be used in prophylactic vaccines against viruses, therapeutic vaccines against cancers and a variety of other emerging therapeutic applications.[22] In addition, pDNA is relatively more stable, more accessible to large-scale production, cheaper to produce and introduces prolonged therapeutic effects in comparison to other nucleic acids.[2,3,20]

To this end, we investigated pDNA transfection efficiency in mice using the three benchmark ionizable cationic lipids developed for the first FDA-approved gene therapy: DODAP, DLin-KC2-DMA and DLin-MC3-DMA. We aimed to learn from the long journey of identifying the optimal ionizable lipid for siRNA delivery (*i.e.*, DLin-MC3-DMA) and design this study is to investigate whether the same characteristics apply to pDNA delivery. Specifically, DODAP, DLin-KC2-DMA and DLin-MC3-DMA were used to encapsulate pDNA encoding a reporter gene in LNPs. The products were administered as intramuscular (IM) or intravenous (IV) injections in mice. Subsequently, gene expression within different mouse organs and tissues was analysed. The results suggested that despite its success with siRNA cargoes DLin-MC3-DMA is not the optimal ionizable lipid for pDNA delivery, providing new insights into the role of ionizable lipids and nucleic acids in organ selectivity and transfection efficiency of LNPs.

2. Materials and methods

2.1 Materials

DLin-MC3-DMA and DLin-KC2-DMA were purchased from DC Chemicals. 1,2-Dioleoyl-3-dimethylammonium-propane (DODAP), distearoylphosphatidylcholine (DSPC), 1,2-dioleoyl-*sn-glycero*-3-phosphocholine (DOPC), 1,2-dioleoyl-*sn-glycero*-3-phospho-ethanolamine (DOPE), and 1,2-distearoyl-*sn-glycero*-3-phosphoethanolamine-*N*-[amino (polyethylene glycol)-2000] (PEG2000-DSPE) were sourced from Avanti Polar Lipids. Cholesterol, L-α-phosphatidylcholine (PC; from egg yolk) and L-α-phosphatidyl-L-serine (PS; from *Glycine max*) were purchased from Sigma Aldrich. All lipids were prepared in 10 mM stocks in 100% ethanol and stored at −20 °C unless otherwise specified. DiI dye was purchased from Thermo Fisher Scientific. Nanoluciferase-CMV1.1 plasmid DNA (NLuc pDNA) was replicated in *E. coli* and purified by PlasmidFactory (Bielefeld, Germany) as research grade DNA and stored at −20 °C prior to use.

2.2 Preparation of LNPs containing NLuc pDNA

NLuc pDNA-LNPs were prepared as previously described.[23] Briefly, the lipid mixture was prepared by mixing specified volumes of ionizable cationic lipids (DODAP, DLin-MC3-DMA, or DLin-KC2-DMA), helper lipids (DSPC or DOPC), cholesterol and a PEG-lipid (PEG2000-DSPE) at a molar ratio of 52/8/38.5/1.5 (mol%), respectively, to form a total final lipid concentration of 10 mM. For the aqueous mixture, pDNA expressing nanoluciferase (NLuc pDNA) was diluted with nuclease-free water to the desired concentration of pDNA, and the pH of the aqueous solution was adjusted to pH 4 using 25 mM sodium acetate buffer. The concentration of the pDNA in the aqueous mixture was determined using a NanoDrop (Nd 3300 Fluorospectrometer, Thermo Fisher Scientific) and adjusted to the desired ionizable cationic lipid to pDNA (N/P) ratio (mol/mol) of the final solution. The aqueous and lipid phases were mixed utilizing a microfluidic chip with a staggered herringbone mixer (SHM) (Precision NanoSystems). The mixing process was carried out on a NanoAssemblr Benchtop system (Precision Nanosystems) at a flow rate ratio of 3 : 1, aqueous : lipid (v/v; respectively), and a total flow rate of 8 mL min^{-1}. The resultant mixture was subsequently purified by dialyzing against phosphate buffered saline (PBS) at pH 7.4 using Pur-A-Lyzer™ Maxi Dialysis Kit (0.1–3 mL, MWCO 6–8 kDa; Sigma Aldrich) for 18–20 h at room temperature. The LNP samples were stored at 4 °C. LNPs used for *in vivo* studies were further filtered (Millex 13 mm Durapore PVDF 0.45 μm; Merck) and concentrated (Amicon Ultra-0.5 mL Centrifugal Filters 50 K; Merck) to a final pDNA concentration of 200 μg mL^{-1} before storing at 4 °C until use.

2.3 LNP characterization

Hydrodynamic size and zeta potential measurements were carried out using dynamic light scattering (DLS) (Zetasizer Nano ZS, Malvern Instruments). Briefly, DLS was used to determine the average particle hydrodynamic size (average particle diameter in nm based on light scattering by intensity) with ZEN0040 disposable cuvettes (Malvern Panalytical) in PBS at a pH of 7.4. For zeta potential measurements, LNPs were diluted 10-fold with nuclease-free water and analyzed using a DTS107 disposable folded capillary (Malvern Panalytical, Malvern, UK). LNP encapsulation efficiency (EE%) of pDNA was quantified using a Quant-iT™ PicoGreen® dsDNA assay kit (Thermo Fisher Scientific). First, the assay buffer was prepared by diluting the Tris-EDTA (TE) buffer 20-fold with DNase-free water to prepare 1× TE working solution. Second, aqueous working solution of the Quant-iT™ PicoGreen® was prepared by diluting the reagent 200-fold using 1× TE buffer. To determine the amount of unencapsulated pDNA (F1), the LNP sample was diluted 50× in TE buffer, then 100 μL was added to one well of a 96-well plate (Corning® 96 Well Solid Polystyrene Microplate). To determine the total pDNA in the LNP sample (F0), LNPs were lysed using 2 μL of 10% Triton X-100, which was added to 100 μL of the LNP solution (50-fold diluted with 1× TE buffer) in an Eppendorf tube and incubated at 40 °C for 15 min with continuous mixing at 300 rpm using a Thermomixer R (Eppendorf). The lysed LNP solution was then transferred to another well of the same microplate. 100 μL of Quant-iT™ PicoGreen® aqueous working solution was added to each well, and the plate was incubated at room temperature for a further 5 min with continuous shaking. The fluorescence intensity was measured using an EnVision 2103 Multilabel Reader (PerkinElmer) at excitation and emission wavelengths of 480 and 520 nm, respectively. To calculate the EE% of the NLuc pDNA in the LNP, the following equation was used:

$$\mathrm{EE}\% = (\mathrm{F0} - \mathrm{F1})/\mathrm{F0} \times 100$$

where F0 equals total pDNA in solution (after LNP lysis), and F1 equals unencapsulated DNA.

Three replicates of each sample were measured to obtain the average EE% measurement. The mean EE% and SD recorded in this study were obtained from independent experiments to confirm the reproducibility of the LNP formulations.

2.4 Cryogenic transmission electron microscopy (cryo-TEM)

Sample preparation for cryo-TEM was undertaken using a FEI Vitrobot Mark IV system. Briefly, systemic humidity was set at 100% and temperature at 4 °C. QuantiFoil® holey carbon or lacey carbon grids were glow-discharged, then 3.5 μL of LNP sample (20-fold concentrated) was applied to grids within the Vitrobot apparatus. One blot step of 3.5 s was carried out with a blotting force of −3, with sample then immediately plunged into liquid ethane. Vitrified samples were stored in liquid nitrogen until use. Samples were imaged on a Tecnai Spirit 200 kV transmission electron microscope utilizing Gatan Microscopy Suite software.

2.5 *In vivo* gene expression of NLuc

BALB/c mice aged 6–12 weeks (weight range of 20–30 g) were allowed to acclimatize for at least one week. Animals were housed on a 12 h light/dark cycle, at ambient temperatures (21–22 °C) and maintained on a standard diet with free access to water. On the day of the experiment, each mouse was anaesthetized by 1–4% isoflurane *via* inhalation prior to receiving a single dose of 10 μg of NLuc pDNA (50 μL) encapsulated in LNPs suspended in PBS buffer (pH 7.4), *via* IV into the tail vein or IM into the calf muscle. Mice were sacrificed 24 h post-injection and organs were harvested by dissection and frozen (−80 °C) until further processing. All experiments were approved by the Monash Institute of Pharmaceutical Sciences, Monash University, animal ethics committee and were conducted in accordance with the Australian and New Zealand Council for the Care of Animals in Research and Teaching guidelines (The approved code is 2021-20345-54900, 27 May 2019).

2.6 Analysis of NLuc gene expression *in vivo* using the nanoluciferase (NLuc) assay

The Nano-Luciferase (NLuc) assay was used to quantify *in vivo* nanoluciferase expression mediated by LNP-encapsulated NLuc pDNA based on the relative luminescence in each tissue, as previously described.[23] Briefly, tissue samples were weighed and transferred to MACS M tubes (Miltenyi Biotech) and 1 mL Glo-lysis buffer (Promega) was added to each tube, then homogenized using a Gentle MACS Octo Dissociator (Miltenyi Biotech) running a standard program (program Protein 1, M-tube mode). Tissue samples were then centrifuged at 3000*g* for 5 min at 4 °C. The supernatants of tissue samples were collected and centrifuged again at 10 000*g* for 5 min at 4 °C to ensure no tissue was present. The supernatants were weight normalized to the same mass of tissue to validate that any variance in luminescence observed between samples is purely due to differences in protein expression. A volume of 100 μL of the tissue lysates and 100 μL of the NLuc reagent (Promega N1130) were added to a 96 well plate (OptiPlate-96 White Microplate; PerkinElmer). Samples in the plate were mixed at ambient temperature, 300 rpm for 15 min. Then, NLuc expression in tissues was analyzed using an EnVision 2103 Multilabel Reader (PerkinElmer) at 460 nm. Relative luminescence units (RLU) were converted and normalized to the amount of NLuc enzyme per mg of the tissue.

2.7 *Ex vivo* bioluminescence imaging

Bioluminescence imaging was performed on isolated organs using the *In Vivo* Imaging System Lumina (IVIS) Lumina II imaging system (PerkinElmer) to measure whole-organ luminescence, as previously described.[23] BALB/c mice aged 6–9 weeks were injected with NLuc pDNA-LNPs IV or IM. After 24 h, tissues were collected and washed with 1× PBS buffer. The Furimazine reagent (Nano-Glo® Luciferase assay substrate; Promega) was prepared by diluting Nano-Glo substrate 40-fold into 1× PBS buffer. Tissues were soaked in the reagent

for 5 min and imaged with an open filter and acquisition times of 1 min. Luminescence data was processed with Living Image 4.3.1 software and expressed as average radiance units of photons per second per centimetre squared per steradian (p s^{-1} cm^{-2} sr^{-1}).

2.8 *In vivo* biodistribution of LNPs

6–9 weeks BALB/c mice were injected IV or IM with NLuc pDNA-LNPs labelled with DiI (0.2 mol% of total lipid in formulation; Thermo Fisher Scientific). After 24 h, mice were sacrificed and tissues were collected and imaged using the *In Vivo* Imaging System Lumina (IVIS) Lumina II imaging system (PerkinElmer). DiI fluorescence intensity was measured at 551 nm excitation/569 nm emission using Living Image 4.3.1 software with and quantified within the region of interest (ROI) for each tissue. Fluorescence data were expressed as average total flux units of photons per second (p s^{-1}).

2.9 *In vitro* endosome escape model assay

To study the capacity of different ionizable lipids to facilitate pDNA release from LNPs within an endosomal compartment, anionic liposomes were utilized to model the endosomal environment.[24–26] PC-DOPE-PS liposomes (6 : 3 : 1 molar ratio) were prepared by dissolving lipids in a chloroform/methanol solution (50 : 50) and generating a lipid film under vacuum at 68 °C. The dried lipid film was then resuspended in 1× PBS (pH 7.4). The anionic liposome mixture was diluted 10-fold by Quant-iT™ PicoGreen® aqueous solution (200-fold diluted using 1× TE buffer) with or without (control, pH 7.2) 10 mM acetate buffer (pH 5.5), then 100 μL was mixed with each LNP sample (50-fold diluted with TE buffer) and transferred to a 96 well plate (Corning® 96 Well Solid Polystyrene Microplate). The samples were added in triplicate into wells and incubated at room temperature for 5 min. Fluorescence intensity of the PicoGreen® dye was measured using an EnVision 2103 Multilabel Reader (PerkinElmer) at excitation and emission wavelengths of 480 and 520 nm, respectively. The amount of pDNA is quantified using a calibration curve (Fig. S1†). DNA release data are presented in Table S1.†

2.10 Statistical analysis

Statistical analyses were performed using GraphPad Prism, version 8.0.2(263). Where applicable, *t*-tests (nonparametric), one or two-way ANOVAs (with the Bonferroni multiple comparisons test) were performed. Data were considered statistically significant if $p < 0.05$.

3. Results and discussion

3.1 Synthesis of LNPs

We first prepared LNPs encapsulating pDNA using DODAP, DLin-KC2-DMA or DLin-MC3-DMA as the ionizable cationic lipid. Cationic lipid is the main component in any LNPs encapsulating nucleic acids (*e.g.*, siRNA, mRNA or pDNA).[27,28] These genetic materials exhibit negative charges on their phosphate backbone and therefore bind to the positively charged cationic lipids.[6] In the first generations of LNPs, permanently positive-charged lipids such as 1,2-dioleoyl-3-trimethylammoniumpropane (DOTAP) were often used to bind nucleic acids and encapsulate them inside LNPs.[29,30] However, permanently positive-charged lipids are not well tolerated *in vivo* and exhibit low transfection efficiency due to their limited ability to release nucleic acid cargos into the cell cytosol or nucleus.[31–33] To address this issue, ionizable cationic lipids such as DODAP were developed (Fig. 1A).[13] Most DODAP molecules are protonated and positively charged at low pH (around 4.0) and hence can bind with nucleic acids, but at physiological pH 7.4 only a small portion of their amines are protonated.[34] As a result, using the ionizable lipid DODAP usually leads to LNPs with a slightly negative surface at physiological pH, thus reducing toxicity and enhancing the number of nucleic acids that can be released into cells.[35,36] We therefore chose DODAP as the first ionizable lipid to investigate in this work. The second ionizable lipid selected was DLin-KC2-DMA, another critical benchmark in the development of LNPs for clinical applications (Fig. 1A).[4] DLin-KC2-DMA has two double bonds per alkyl chain instead of one in DODAP. Thanks to the increase in the unsaturated level of its lipid tail, DLin-KC2-DMA exhibited significantly high siRNA gene silencing efficiency.[15] The final lipid studied in this work was DLin-MC3-DMA, an optimized ionizable lipid used in the FDA-approved product Onpattro (Fig. 1A). DLin-MC3-DMA has an identical lipid tail to DLin-KC2-DMA but possesses a different head group.[16] By selecting these benchmark ionizable lipids, we aimed to ask whether the efficiency of these lipids for delivery of pDNA correlates with what was reported during the development of the first FDA-appoved siRNA therapy Onpattro.

Aside from the ionizable lipid, other lipid components and ratios were kept identical across all formulations to enable meaningful comparison (Fig. 1B). In particular, cholesterol was employed to enhance LNP stability and promote endosomal escape.[37] DSPC was used as a helper lipid to facilitate the formation of LNPs.[38] PEG-conjugated DSPE was employed to anchor on the surface of LNPs and stabilize them through steric hindrance.[39] The molar ratio of ionizable lipid : cholesterol : DSPC : PEG-DSPE was kept constant at a previously optimized ratio of 52 : 38.5 : 8 : 1.5, respectively.[23] All LNP components were dissolved in ethanol and injected into one inlet of a microfluidic chip (NanoAssemblr), which was specially designed for scalable, rapid, and reproducible preparation of LNPs (Fig. 1C).[40] pDNA encoding for a reporter gene nanoluciferase (NLuc) was solubilized in acetate buffer (pH 4) and injected simultaneously into the second inlet to facilitate primary LNP formation. We selected NLuc as the reporter gene because NLuc produces nearly a hundred times brighter luminescence than luciferase providing good signals for both imaging and quantification of DNA transfection efficiency.[23] The primary LNP mixture was collected from the outlet and dialyzed against PBS buffer (pH 7.4) to increase the solution pH and form the finished LNPs.

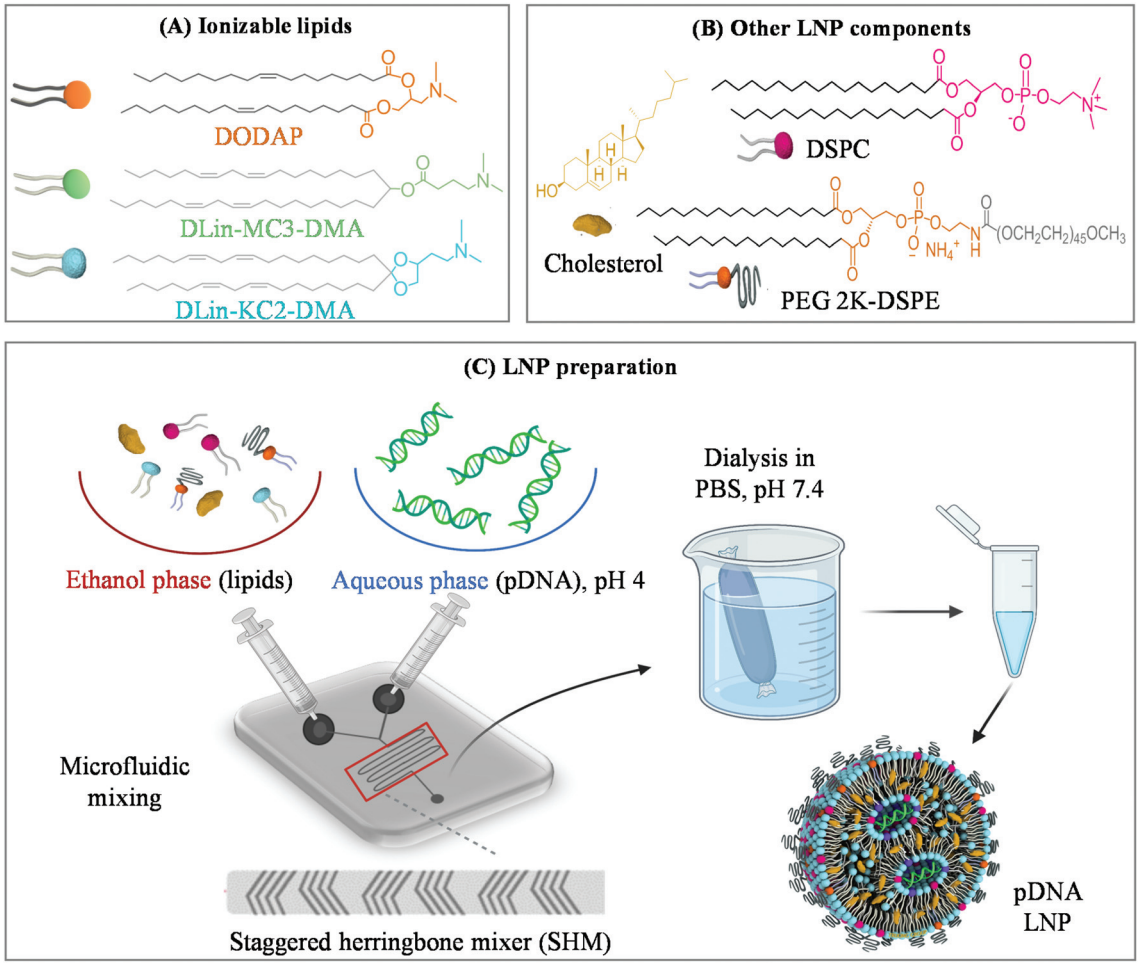

Fig. 1 Chemical and representative cartoon structures of (A) the three ionizable lipids utilized in LNP formulations (DODAP, DLin-MC3-DMA and DLin-KC2-DMA) and (B) other components used for all LNP formulations (DSPC, cholesterol, and PEG2000-DSPE). (C) Preparation of LNPs by a simple, rapid, reproducible and scalable microfluidic technology. Created with BioRender.com.

3.2 Characterization of LNPs

After synthesis, DODAP, DLin-KC2-DMA and DLin-MC3-DMA LNPs were comprehensively characterized by dynamic light scattering (DLS), PicoGreen® pDNA encapsulation efficiency assay, and cryogenic electron microscopy (cryo-EM). To determine the optimal amount of ionizable lipids for particle formation and encapsulation of pDNA, we tested three different N/P ratios (*i.e.*, the ratio between the nitrogen group of the ionizable lipids and the phosphate group on the backbone of pDNA). Increasing the N/P ratio from 3 to 6 and 9 led to a significantly smaller size, regardless of the ionizable lipids used (Fig. 2A and Table S2†). It has been reported that most of the anime groups of all three ionizable lipids exhibited a positive charge in acetate buffer (pH 4).[41] Therefore, the strong binding between positively charged ionizable lipids and negatively charged pDNA at a high N/P ratio led to the formation of small compacted LNPs. This result was supported by zeta potential data shown in Fig. 2B: increasing the N/P ratio led to the formation of less negatively charged LNPs. It should also be noted that the zeta potential and size were measured when the LNPs were fully formed in PBS buffer (pH 7.4). At this physiological pH, the ionizable lipid nitrogens were mostly (but not all) deprotonated and neutral while pDNA and PEGylated surface have negative charges. Thus, the zeta potential of LNPs exhibited overall negative values from the pDNA and PEG. Furthermore, polydispersity indices (PDI) of LNPs at N/P 3 were significantly higher than those at N/P 6 and 9 (Fig. 2C). This data suggests that at N/P 3, there are not enough positively charged lipids to complex with all negatively-charged pDNA molecules, resulting in a proportion of the pDNA remaining free in solution.

To confirm this hypothesis, we measured the pDNA encapsulation efficiency (*i.e.*, the percentage of plasmid DNA encapsulated inside LNP comparative to the total amount of pDNA). PicoGreen®, a dye that can produce bright fluorescence when bound specifically to free double-stranded DNA, was added to the LNP solution to quantify the amount of free pDNA not encapsulated within LNPs.[42] Triton X-100 was then used to lyse the LNP and release encapsulated pDNA so that the total

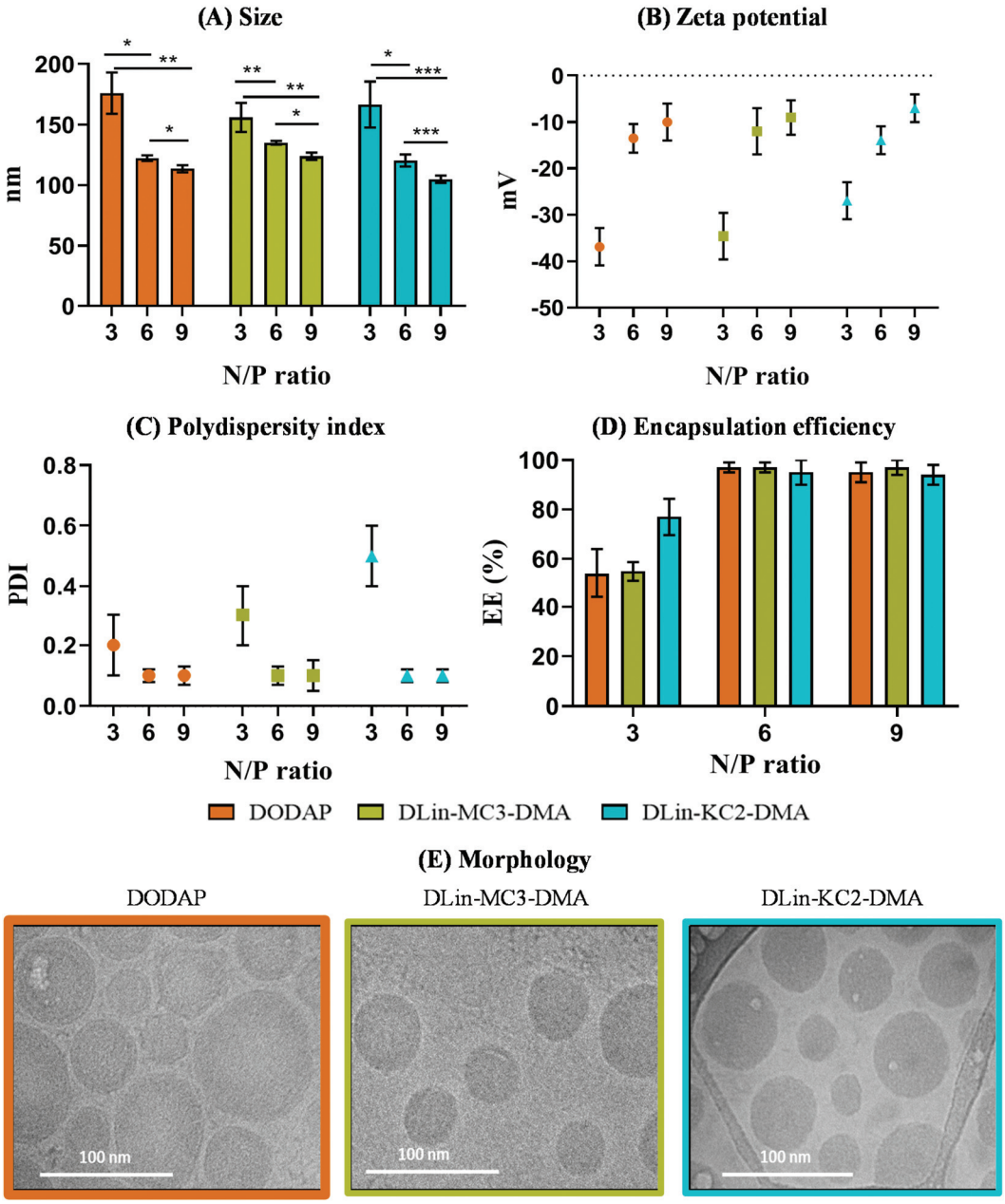

Fig. 2 Characterization of LNPs by DLS showing (A) particle size (hydrodynamic diameter), (B) zeta potential, and (C) polydispersity index (PDI). (D) Encapsulation efficiency (EE%) by PicoGreen® assay. (E) LNP morphology by cryo-TEM. N/P ratio of LNPs in cryo-TEM images is 6. For (A), * $p < 0.05$; ** $p < 0.01$; *** $p < 0.001$ as determined using an unpaired t-test comparing size at various N/P ratios for each formulation.

amount of DNA could be determined and the encapsulation efficiency could be calculated.[43] As shown in Fig. 2D, the encapsulation efficiency of all LNPs at N/P 3 was around 60% to 70%, which is lower than that at higher N/P ratios (more than 90%). The presence of unencapsulated pDNA at N/P 3 was in good agreement with the highly negative zeta potential and high PDI at this N/P ratio, confirming the presence of unencapsulated pDNA. We chose N/P 6 for further experiments due to LNPs formed at this ratio exhibiting particle sizes suitable for *in vivo* gene delivery (~120 nm), low polydispersity (~0.1), and high encapsulation efficiency (>90%). A higher N/P ratio of 9 increases the zeta potential and is expected to reduce the pDNA release capacity causing low transfection efficiency of LNPs.[44,45] We next employed cryo-EM to characterize LNPs directly in solution (rather than in a dehydrated state per TEM), and the results indicate that all LNPs have a comparable spherical morphology comprised of packed lipid complexes (Fig. 2).[46] Taken together, the characterization results demonstrate that using the three different ionizable lipids to encapsulate pDNA results in LNPs with comparable properties, allowing us to directly compare their *in vivo* transfection efficiency without the confounding effect of different physicochemical properties.

3.3 *In vivo* transfection *via* IM administration

After synthesis and characterization, we next investigated *in vivo* pDNA transfection in different mouse organs *via* IM administration, a route widely used for vaccine application. DODAP, DLin-KC2-DMA and DLin-MC3-DMA LNPs were first injected into the calf muscle of mice. 24 h after injection, eight organs were harvested, including the draining lymph nodes (DLN), non-draining lymph nodes (nDLN), calf muscle (MC), heart (HT), lung (LG), liver (LV), spleen (SP), and kidneys (KD). We first employed *In Vivo* Imaging System (IVIS, Lumina II) to observe the expression of NLuc proteins in these organs by incubating them with Furimazine (Fig. 3A). This reagent can react specifically with NLuc proteins produced *in vivo* to emit luminescence across a color spectrum representing the relative level of protein expression (*i.e.* red indicates more NLuc protein produced than yellow, green, and blue).[47] The result in Fig. 3A shows that 24 h post-IM administration, pDNA from all three LNPs was transfected mainly in the calf muscle, *i.e.* the injection site. A small proportion of DLin-KC2-DMA LNPs was able to transfect both draining and non-draining lymph nodes as weak luminescence signals were observed in these tissues. Interestingly, DLin-MC3-DMA LNPs exhibited low transfection in the DLN, but negligible signal was found in the nDLN. DODAP LNPs did not effectively deliver pDNA beyond the injection site, as no luminescence was observed in all other organs. This data indicates that both the transfection efficiency and tissue localization of DODAP, DLin-KC2-DMA and DLin-MC3-DMA LNPs is affected by the type of ionizable lipid used. However, from the IVIS images, quantification of proteins produced was unable to be performed and hence, the performance of different ionizable lipids, especially in the muscle, cannot be determined.

Therefore, we further quantified the transfection efficiency of these LNPs by homogenizing these organs and measuring the luminescence signals as a relative light unit (RLU). It should be noted that homogenizing the organs allowed better quantitative measurement of NLuc protein concentration, and the data presented in Fig. 3B and Table S3† were obtained from five independent experiments (instead of one in the IVIS study). We also normalized the data as RLU per mg of tissue to compare the transfection efficiency in different organs without the confounding effect of variation in tissue mass (for example, the muscle is larger by weight than the lymph nodes and has more cells, so without normalization, a higher RLU may be observed even with a lower transfection efficiency). Interestingly, the data in Fig. 3B showed that DLin-KC2-DMA LNPs exhibited the highest *in vivo* transfection efficiency even when compared to the previously known best-performing ionizable lipid DLin-MC3-DMA. Although there was no statistically significant difference in pDNA transfection between DLin-KC2-DMA and DLin-MC3-DMA LNPs in the DLN, more than two and five times higher transfection efficiency was found for DLin-KC2-DMA LNPs in the muscle and nDLN, respectively. On the other hand, DODAP LNPs had the lowest transfection efficiency among the ionizable lipids used. Altogether, this study suggests that when compared with DODAP and DLin-MC3-DMA, DLin-KC2-DMA is a more effective ionizable lipid for *in vivo* pDNA transfection *via* IM administration, which is a significant finding for specific applications such as DNA vaccination where IM administration is a prefered injection route. This finding was surprising but not necessarily in contrast to the previous work reporting Dlin-MC3-DMA was the optimum ionizable lipid for siRNA delivery *via* IV injection.[16] As the injection route may also affect the delivery efficiency of LNPs, we were also interested in investi-

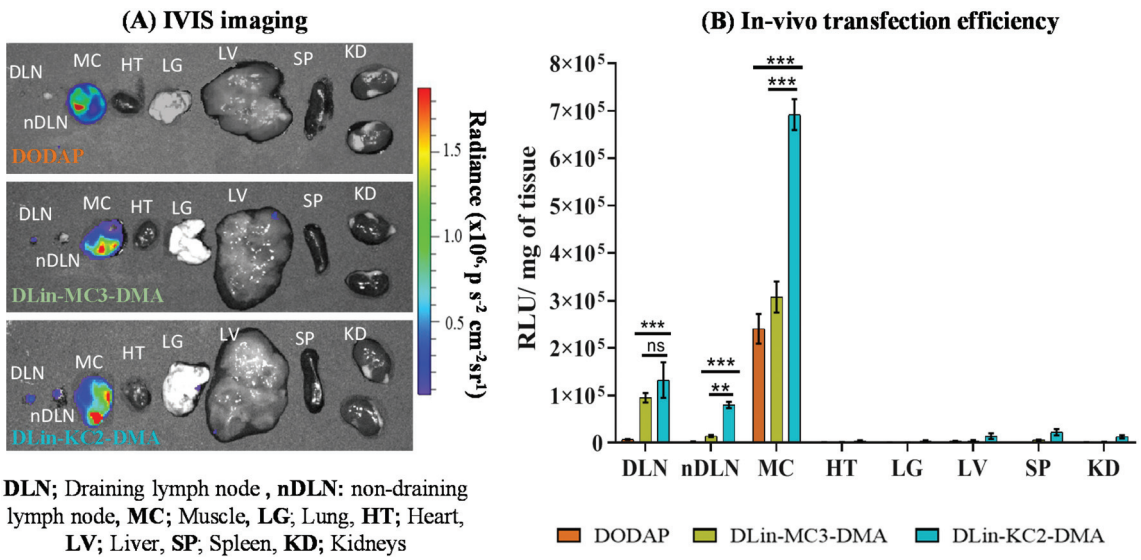

Fig. 3 NLuc expression 24 h after IM of pDNA LNPs using (A) IVIS imaging and (B) NLuc quantification assay. Results represent mean ± SEM of independent experiments (n = 5). The symbols indicate p-values ns (p = 0.12), ** p < 0.01; *** p < 0.001 as determined using an ANOVA analysis with a Bonferroni multiple comparisons test.

gating the transfection efficiency of these LNPs *via* IV administration (Fig. S2†).

3.4 *In vivo* transfection *via* IV administration

For IV administration, DODAP, DLin-MC3-DMA and DLin-KC2-DMA LNPs with the NLuc pDNA cargo were injected into the tail vein of mice. By IV injection, LNPs were expected to enter the blood circulation and access more organs and tissues than by IM injection.[48] Indeed, IVIS images in Fig. 4A show that all LNPs were capable of transfecting cells in the majority of the organs studied, including the heart, lungs, liver, spleen, kidneys and inguinal lymph nodes (iLN). Surprisingly, we observed strong (red) signals in the spleen for both DLin-KC2-DMA and DLin-MC3-DMA LNPs. Further quantification of the transfection efficiency *via* organ homogenization confirmed significant expression of NLuc in the spleen mediated by DLin-KC2-DMA LNPs. DLin-MC3-DMA LNPs also expressed more NLuc proteins in the spleen than in any other organ (Fig. 4B and Table S4†). Interestingly, we observed the same trend of transfection efficiency as with IM injection: DLin-KC2-DMA LNPs exhibited the overall highest transfection efficiency comparative to the other ionizable lipid formulations. For example, DLin-KC2-DMA LNPs had approximately 3-fold and 13-fold higher transfection efficiency in the spleen than DLin-MC3-DMA and DODAP LNPs, respectively.

Notably, DLin-KC2-DMA LNPs still transfected much more efficiently than DODAP and DLin-MC3-DMA LNPs even in the liver. Compared to DODAP, the higher transfection efficiency of DLin-KC2-DMA LNPs in the liver is analogous to its siRNA gene silencing performance. However, the superior performance in the liver of DLin-KC2-DMA compared to DLin-MC3-DMA is surprising, given that DLin-MC3-DMA LNPs such as Onpattro was designed for targeted delivery of siRNA to the liver after IV administration. That said, this result is in agreement with their *in vitro* DNA transfection in cancer cell lines and *in vivo* DNA transfection in a special chicken embryo model.[49] Interestingly, only DLin-KC2-DMA LNPs could transfect in the iLN and KD, although the efficiency was relatively low. Furthermore, DLin-MC3-DMA surprisingly expressed more proteins in the spleen than in the liver. This result suggests that not only the ionizable lipid but also the nucleic acid itself contributed to different transfection efficiency in different organs. In addition, DLin-KC2-DMA and DLin-MC3-DMA LNPs have higher transfection in the spleen compared to in the liver.

Notwithstanding these exciting and significant findings above, it remains unclear whether the high transfection efficiency of DLin-KC2-DMA and DLin-MC3-DMA LNPs is related to other contributing factors, such as (a) more LNPs accumulated in the spleen or (b) the higher transfection efficiency of LNPs occurred in this organ. This question was particularly important when in this work we employed PEG conjugated to a longer lipid tail (PEG-DSPE; 18C chain) than in the Onpattro formulation (PEG-DMG; 14C chain) as it has been documented that the short lipid tail of the PEG can result in high liver accumulation.[50,51] In addition, as DLin-KC2-DMA has an identical lipid tail to DLin-MC3-DMA, we hypothesized that the difference in the head group length and pK_a might affect the interaction between the ionizable lipid and endosomal membrane, leading to different endosome escape outcomes and pDNA release capacity. To clarify these two remaining unclear points, we next performed *in vivo* biodistribution and *in vitro* endosome escape studies.

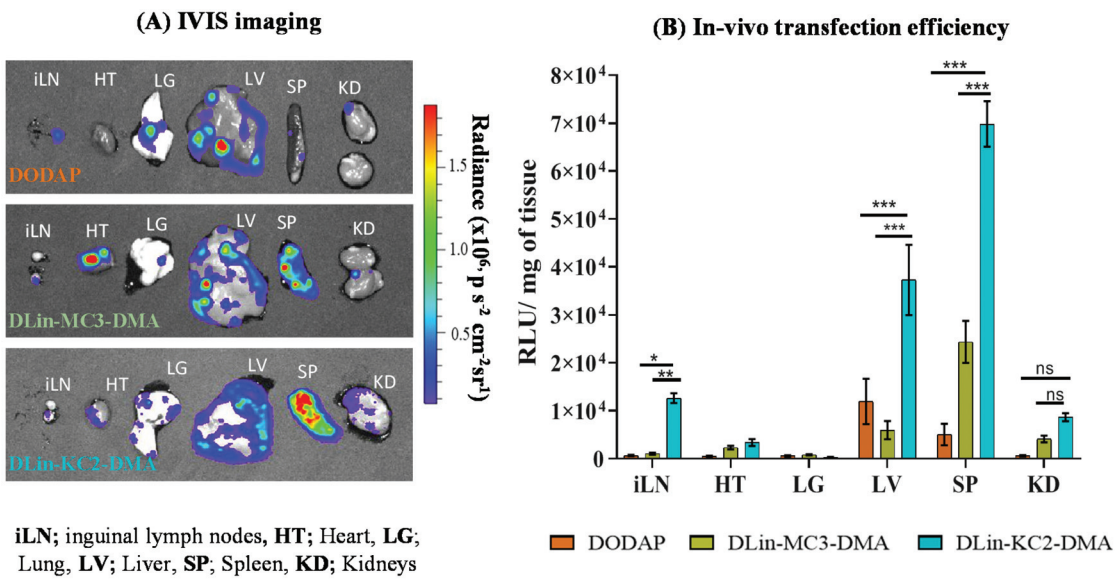

Fig. 4 NLuc expression of pDNA 24 h after IV of LNP-pDNA using (A) IVIS imaging and (B) NLuc quantification assay. Results represent mean ± SEM of independent experiments (n = 5). The symbols indicate p-values ns (p = 0.12), * p < 0.05; ** p < 0.01; *** p < 0.001 as determined using an ANOVA analysis with the Bonferroni multiple comparisons test.

3.5 *In vivo* biodistribution and *in vitro* endosome escape

A hydrophobic fluorescent dye was intercalated into the LNPs to track their biodistribution in different organs 24 h after the IV or IM injection, and therefore to probe differences in particle accumulation between DLin-KC2-DMA and DLin-MC3-DMA LNPs. DiI was selected as a suitable dye due to bright fluorescence and the presence of two very long lipid tails, making it unlikely to detach from LNPs during circulation.[51,52] All other components of LNPs remained unchanged. The results of the *in vivo* biodistribution study in Fig. 5 reveal that all LNPs accumulated mainly in the liver, regardless of the administration route or ionizable lipid used. Aside from the liver, LNPs also accumulated in the kidneys and lung after IV administration, while for IM injection, LNPs additionally localized to the muscle and lung. There was little fluorescent signal in other organs, such as the spleen. These interesting data indicated that the high transfection efficiency in the spleen and muscle for the IV and IM routes was not directly correlated to the biodistribution of LNPs. High *in vivo* transfection in the spleen while accumulation occurred mainly in the liver has also been shown for other LNP formulations.[53,54] The data indicate that high transfection efficiency in different organs is related to the expression of nucleic acid and the endosomal escape driven by the ionizable lipid rather than the biodistribution of LNPs. This work shows that in the context of nucleic acid nanoparticles, studying the ultimate gene expression of the formulated nucleic acids is a better indicator than nucleic acid fate and biodistribution. Moreover, this work paves the way for new studies to fully understand this characteristic and explore it for new applications such as immunotherapies, whereby high gene expression in the spleen is hugely beneficial.

Finally, we performed a well-established *in vitro* endosomal escape model assay[24–26] to examine our hypothesis that differences in the head and tail between DLin-MC3-DMA and DLin-KC2-DMA could result in different endosome escape outcomes and DNA release capacity of LNPs. The interaction between LNP lipids and the endosomal membrane is one of the most vital steps in the effective delivery of a pDNA cargo.[2] It facilitates the escape of the pDNA from the acidic, DNA-degradable endosomal compartment to the physiological environment of the cytosol, allowing further translation of the pDNA to occur once it reaches the nucleus.[55] In this widely used assay, a negatively charged liposome is used to mimic the endosome membrane and interact with LNPs.[24–26] The ionizable lipids of LNPs are expected to become protonated only at low endosomal pH (5.5) and interact with the anionic charges of the liposome, allowing the release of the entrapped pDNA.[56] PicoGreen® dye was also utilized to quantify the amount of free pDNA in the LNP solution at physiological pH 7.4 and endosomal pH 5.5, allowing us to calculate the amount of pDNA being released from the LNPs when the environmental pH is changed.

The data presented in Fig. 6 demonstrates that DLin-KC2-DMA indeed performs significantly better in simulating endosomal escape and release of pDNA comparative to DLin-MC3-

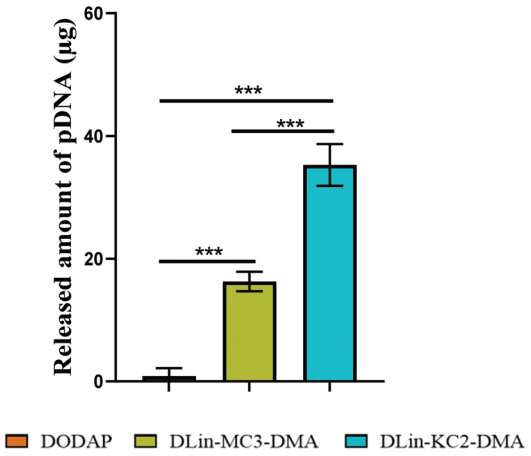

Fig. 6 Measurement of pDNA release from LNPs at pH 5.5 by a model *in vitro* endosomal escape assay. Data represented as mean ± SD (n = 3). Statistical significance was determined using a one-way ANOVA; *** indicates $p < 0.001$.

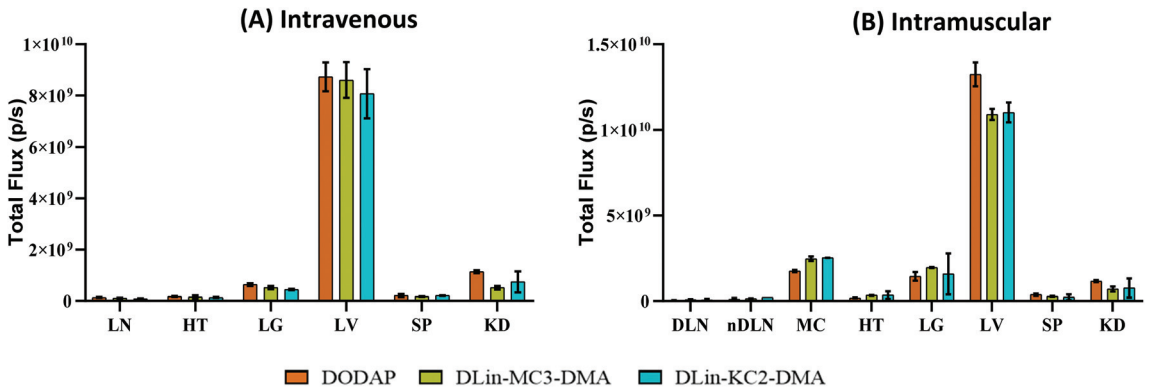

Fig. 5 Biodistribution of fluorescently labelled LNPs. LNPs were labelled with DiI dye and administered (A) intravenously or (B) intramuscularly. Tissues were collected and DiI fluorescence as total flux (p s^{-1}) in each was obtained using IVIS after 24 h. Data are presented as mean with SD (n = 3). LN: lymph node; HT: heart; LG: lung; LV: liver; SP: spleen; KD: kidneys.

DMA and DODAP. DLin-KC2-DMA and DLin-MC3-DMA both likely facilitated better endosomal escape than DODAP in this model system probably due to their two unsaturated bonds per lipid tail, which favours the formation of an inverted hexagonal (H_{II}) phase.[57] The intermediate H_{II} phase seems to be essential for the fusion between the LNP and endosomal membrane.[58] The fusion does not only destabilizes the endosomal membrane but also disassembles the LNPs and releases encapsulated pDNA.[58] On the other hand, DODAP has only one unsaturated bond per tail, which does not support the intermediate H_{II} phase formation, likely leading to the low level of endosomal escape and DNA release observed.[2] In addition to having suitable unsaturated lipid tails for membrane fusion, the DLin-KC2-DMA head group has a higher pK_a (6.7)[15] than DLin-MC3-DMA (6.4).[16] It's conceivable that at pH 5.5, a higher number of head groups are protonated with DLin-KC2-DMA. The positively charged head groups are needed to form ion pairs with the anionic lipids of the endosomal membrane, triggering the formation of the H_{II} phase and membrane fusion.[58] Taken together, DLin-KC2-DMA may have preferential endosome escape and release of pDNA, resulting in high *in vivo* transfection efficiency. Notably, DLin-MC3-DMA formulations have been reported to have higher gene silencing efficiency in the liver (*i.e.*, more effective delivery of siRNA) than DLin-KC2-DMA.[15] The difference can be attributed to the nature of siRNA and pDNA: siRNA has a much shorter negatively-charged backbone, which interacts with fewer positively-charged head groups of the ionizable lipid than pDNA.[17] Therefore, DLin-MC3-DMA, with a lower pK_a and fewer charged head groups, is more suitable for siRNA than DLin-KC2-DMA. On the other hand, using DLin-KC2-DMA with more charged head groups for siRNA may increase its interaction with not only the endosome membrane but also with siRNA molecules, thus reducing the amount of siRNA being released. Interestingly, small differences in pK_a and length of the head group regarding DLin-MC3-DMA and DLin-KC2-DMA do not appear to affect the biodistribution of LNPs, but strongly affect the *in vivo* transfection efficiency of LNPs. Lastly, the differences in gene expression may be also attributed to the particle size of DLin-MC3-DMA and DLin-KC2-DMA LNPs. The size of siRNA LNPs is generally in the average of 50–100 nm, smaller than pDNA LNPs. Previous studies showed that silencing liver enzymes is predominatly driven at lower particle sizes, and that silencing is reduced with increasing particle size.[51] Altogether, these data confirm the importance of ionizable lipid structure in *in vivo* gene expression.

4. Conclusions

This work reports the first systematic comparison of pDNA transfection efficiency in mouse organs for three ionizable lipids including one used in the first FDA-approved siRNA therapeutic Onpattro. We found that DODAP, DLin-KC2-DMA and DLin-MC3-DMA ionizable lipids could facilitate the formation of relatively uniform LNPs exhibiting high pDNA encapsulation efficiency at an N/P ratio of 6. These formulated LNPs shared similar physicochemical properties but exhibited very different levels of gene expression depending on the ionizable lipid used and the administration route. Interestingly, LNPs prepared from DLin-KC2-DMA had overall higher *in vivo* DNA transfection efficiency than DLin-MC3-DMA and DODAP when administered to mice *via* both IV and IM. Furthermore, the muscle was the main organ transfected after IM administration of all LNPs. However, the spleen rather than the liver displayed the highest levels of transfection after IV injection. The transfection efficiency was correlated mainly to the ionizable lipid structure rather than to the biodistribution of the LNPs. In particular, the unsaturated level of the tail and the pK_a of the head group significantly was shown to significantly affect endosomal escape and DNA release. This study suggests that the selection of ionizable lipid for specific nucleic acid cargo can be critical to maximizing therapeutic outcomes and that DLin-KC2-DMA is superior to other benchmark ionizable lipids for the effective delivery of pDNA when particles share similar physiochemical properties. Our work will guide the design of novel pDNA LNPs for various fundamental research and medical applications, such as gene editing, immunotherapies vaccines, and protein replacement therapies.

Conflicts of interest

There are no conflicts of interest to declare.

Acknowledgements

N. P. T. acknowledges the receipt of a Discovery Project grant (DP200100231), a Discovery Early Career Researcher Award (DE180100076) from the Australian Research Council (ARC) and an Ideas grant (APP2002827) from the National Health and Medical Research Council (NHMRC).

References

1 L. Naldini, Gene therapy returns to centre stage, *Nature*, 2015, **526**, 351–360.
2 E. Samaridou, J. Heyes and P. Lutwyche, Lipid nanoparticles for nucleic acid delivery: Current perspectives, *Adv. Drug Delivery Rev.*, 2020, **154-155**, 37–63.
3 J. A. Kulkarni, D. Witzigmann, S. B. Thomson, S. Chen, B. R. Leavitt, P. R. Cullis and R. van der Meel, The current landscape of nucleic acid therapeutics, *Nat. Nanotechnol.*, 2021, **16**, 630–643.
4 A. Akinc, M. A. Maier, M. Manoharan, K. Fitzgerald, M. Jayaraman, S. Barros, S. Ansell, X. Y. Du, M. J. Hope, T. D. Madden, B. L. Mui, S. C. Semple, Y. K. Tam, M. Ciufolini, D. Witzigmann, J. A. Kulkarni, R. van der Meel and P. R. Cullis, The Onpattro story and the clinical translation of nanomedicines containing nucleic acid-based drugs, *Nat. Nanotechnol.*, 2019, **14**, 1084–1087.

5 J. Cohen, Vaccine designers take first shots at COVID-19, *Science*, 2020, **368**, 14–16.
6 E. H. Pilkington, E. J. A. Suys, N. L. Trevaskis, A. K. Wheatley, D. Zukancic, A. Algarni, H. Al-Wassiti, T. P. Davis, C. W. Pouton, S. J. Kent and N. P. Truong, From influenza to COVID-19: Lipid nanoparticle mRNA vaccines at the frontiers of infectious diseases, *Acta Biomater.*, 2021, **131**, 16–40.
7 N. P. Truong, W. Y. Gu, I. Prasadam, Z. F. Jia, R. Crawford, Y. Xiao and M. J. Monteiro, An influenza virus-inspired polymer system for the timed release of siRNA, *Nat. Commun.*, 2013, **4**, 1902.
8 S. B. Hartono, N. P. Truong, M. H. Yu, Z. F. Jia, M. J. Monteiro, S. H. Qiao and C. Z. Yu, Functionalized large pore mesoporous silica nanoparticles for gene delivery featuring controlled release and co-delivery, *J. Mater. Chem. B*, 2014, **2**, 718–726.
9 X. Xu, J. Wu, S. Liu, P. E. Saw, W. Tao, Y. Li, L. Krygsman, S. Yegnasubramanian, A. M. De Marzo, J. Shi, C. J. Bieberich and O. C. Farokhzad, Redox-Responsive Nanoparticle-Mediated Systemic RNAi for Effective Cancer Therapy, *Small*, 2018, **14**, 1802565.
10 X. You, Z. Gu, J. Huang, Y. Kang, C.-C. Chu and J. Wu, Arginine-based poly(ester amide) nanoparticle platform: From structure–property relationship to nucleic acid delivery, *Acta Biomater.*, 2018, **74**, 180–191.
11 T. T. H. Thi, E. J. A. Suys, J. S. Lee, D. H. Nguyen, K. D. Park and N. P. Truong, Lipid-Based Nanoparticles in the Clinic and Clinical Trials: From Cancer Nanomedicine to COVID-19 Vaccines, *Vaccines*, 2021, **9**, 359.
12 M. Das, S. Musetti and L. Huang, RNA Interference-Based Cancer Drugs: The Roadblocks, and the "Delivery" of the Promise, *Nucleic Acid Ther.*, 2019, **29**, 61–66.
13 S. C. Semple, S. K. Klimuk, T. O. Harasym and M. J. Hope, Lipid-based formulations of antisense oligonucleotides for systemic delivery applications, *Methods Enzymol.*, 2000, **313**, 322–341.
14 J. Heyes, L. Palmer, K. Bremner and I. MacLachlan, Cationic lipid saturation influences intracellular delivery of encapsulated nucleic acids, *J. Controlled Release*, 2005, **107**, 276–287.
15 S. C. Semple, A. Akinc, J. Chen, A. P. Sandhu, B. L. Mui, C. K. Cho, D. W. Sah, D. Stebbing, E. J. Crosley, E. Yaworski, I. M. Hafez, J. R. Dorkin, J. Qin, K. Lam, K. G. Rajeev, K. F. Wong, L. B. Jeffs, L. Nechev, M. L. Eisenhardt, M. Jayaraman, M. Kazem, M. A. Maier, M. Srinivasulu, M. J. Weinstein, Q. Chen, R. Alvarez, S. A. Barros, S. De, S. K. Klimuk, T. Borland, V. Kosovrasti, W. L. Cantley, Y. K. Tam, M. Manoharan, M. A. Ciufolini, M. A. Tracy, A. de Fougerolles, I. MacLachlan, P. R. Cullis, T. D. Madden and M. J. Hope, Rational design of cationic lipids for siRNA delivery, *Nat. Biotechnol.*, 2010, **28**, 172–176.
16 M. Jayaraman, S. M. Ansell, B. L. Mui, Y. K. Tam, J. Chen, X. Du, D. Butler, L. Eltepu, S. Matsuda, J. K. Narayanannair, K. G. Rajeev, I. M. Hafez, A. Akinc, M. A. Maier, M. A. Tracy, P. R. Cullis, T. D. Madden, M. Manoharan and M. J. Hope, Maximizing the potency of siRNA lipid nanoparticles for hepatic gene silencing in vivo, *Angew. Chem., Int. Ed.*, 2012, **51**, 8529–8533.
17 P. Vader, L. J. van der Aa, G. Storm, R. M. Schiffelers and J. F. J. Engbersen, Polymeric Carrier Systems for siRNA Delivery, *Curr. Top. Med. Chem.*, 2012, **12**, 108–119.
18 P. R. Cook, Molecular biology - The organization of replication and transcription, *Science*, 1999, **284**, 1790–1795.
19 A. Wittrup and J. Lieberman, Knocking down disease: a progress report on siRNA therapeutics, *Nat. Rev. Genet.*, 2015, **16**, 543–552.
20 J. Buck, P. Grossen, P. R. Cullis, J. Huwyler and D. Witzigmann, Lipid-Based DNA Therapeutics: Hallmarks of Non-Viral Gene Delivery, *ACS Nano*, 2019, **13**, 3754–3782.
21 Z. Zhang, T. Wan, Y. X. Chen, Y. Chen, H. W. Sun, T. Q. Cao, S. Y. Zhou, G. P. Tang, C. B. Wu, Y. Ping, F. J. Xu and J. J. Huang, Cationic Polymer-Mediated CRISPR/Cas9 Plasmid Delivery for Genome Editing, *Macromol. Rapid Commun.*, 2019, **40**, 1800068.
22 R. S. Riley, C. H. June, R. Langer and M. J. Mitchell, Delivery technologies for cancer immunotherapy, *Nat. Rev. Drug Discovery*, 2019, **18**, 175–196.
23 D. Zukancic, E. J. A. Suys, E. H. Pilkington, A. Algarni, H. Al-Wassiti and N. P. Truong, The Importance of Poly (ethylene glycol) and Lipid Structure in Targeted Gene Delivery to Lymph Nodes by Lipid Nanoparticles, *Pharmaceutics*, 2020, **12**, 1068.
24 K. Rombouts, T. F. Martens, E. Zagato, J. Demeester, S. C. De Smedt, K. Braeckmans and K. Remaut, Effect of Covalent Fluorescence Labeling of Plasmid DNA on Its Intracellular Processing and Transfection with Lipid-Based Carriers, *Mol. Pharmaceutics*, 2014, **11**, 1359–1368.
25 Y. H. Xu and F. C. Szoka, Mechanism of DNA release from cationic liposome/DNA complexes used in cell transfection, *Biochemistry*, 1996, **35**, 5616–5623.
26 L. Y. Song, Q. F. Ahkong, Q. Rong, Z. Wang, S. Ansell, M. J. Hope and B. Mui, Characterization of the inhibitory effect of PEG-lipid conjugates on the intracellular delivery of plasmid and antisense DNA mediated by cationic lipid liposomes, *Biochim. Biophys. Acta, Biomembr.*, 2002, **1558**, 1–13.
27 E. Vighi, B. Ruozi, M. Montanari, R. Battini and E. Leo, pDNA condensation capacity and in vitro gene delivery properties of cationic solid lipid nanoparticles, *Int. J. Pharm.*, 2010, **389**, 254–261.
28 H. Zhang, X. You, X. Wang, L. Cui, Z. Wang, F. Xu, M. Li, Z. Yang, J. Liu, P. Huang, Y. Kang, J. Wu and X. Xia, Delivery of mRNA vaccine with a lipid-like material potentiates antitumor efficacy through Toll-like receptor 4 signaling, *Proc. Natl. Acad. Sci. U. S. A.*, 2021, **118**, e2005191118.
29 Q. Cheng, T. Wei, L. Farbiak, L. T. Johnson, S. A. Dilliard and D. J. Siegwart, Selective organ targeting (SORT) nano-

particles for tissue-specific mRNA delivery and CRISPR-Cas gene editing, *Nat. Nanotechnol.*, 2020, **15**, 313–320.
30 N. S. Templeton, D. D. Lasic, P. M. Frederik, H. H. Strey, D. D. Roberts and G. N. Pavlakis, Improved DNA: Liposome complexes for increased systemic delivery and gene expression, *Nat. Biotechnol.*, 1997, **15**, 647–652.
31 R. Kedmi, N. Ben-Arie and D. Peer, The systemic toxicity of positively charged lipid nanoparticles and the role of Toll-like receptor 4 in immune activation, *Biomaterials*, 2010, **31**, 6867–6875.
32 A. Gordillo-Galeano and C. E. Mora-Huertas, Solid lipid nanoparticles and nanostructured lipid carriers: A review emphasizing on particle structure and drug release, *Eur. J. Pharm. Biopharm.*, 2018, **133**, 285–308.
33 M. N. Vu, H. G. Kelly, A. K. Wheatley, S. Peng, E. H. Pilkington, N. A. Veldhuis, T. P. Davis, S. J. Kent and N. P. Truong, Cellular Interactions of Liposomes and PISA Nanoparticles during Human Blood Flow in a Microvascular Network, *Small*, 2020, **16**, 2002861.
34 A. L. Bailey and P. R. Cullis, Modulation of Membrane-Fusion by Asymmetric Transbilayer Distributions of Amino Lipids, *Biochemistry*, 1994, **33**, 12573–12580.
35 C. Lonez, M. Vandenbranden and J. M. Ruysschaert, Cationic liposomal lipids: From gene carriers to cell signaling, *Prog. Lipid Res.*, 2008, **47**, 340–347.
36 Z. U. Rehman, I. S. Zuhorn and D. Hoekstra, How cationic lipids transfer nucleic acids into cells and across cellular membranes: Recent advances, *J. Controlled Release*, 2013, **166**, 46–56.
37 S. Patel, N. Ashwanikumar, E. Robinson, Y. Xia, C. Mihai, J. P. Griffith, S. G. Hou, A. A. Esposito, T. Ketova, K. Welsher, J. L. Joyal, O. Almarsson and G. Sahay, Naturally-occurring cholesterol analogues in lipid nanoparticles induce polymorphic shape and enhance intracellular delivery of mRNA (vol 11, 983, 2020), *Nat. Commun.*, 2020, **11**, 983.
38 X. W. Cheng and R. J. Lee, The role of helper lipids in lipid nanoparticles (LNPs) designed for oligonucleotide delivery, *Adv. Drug Delivery Rev.*, 2016, **99**, 129–137.
39 T. T. H. Thi, E. H. Pilkington, D. H. Nguyen, J. S. Lee, K. D. Park and N. P. Truong, The Importance of Poly(ethylene glycol) Alternatives for Overcoming PEG Immunogenicity in Drug Delivery and Bioconjugation, *Polymer*, 2020, **12**, 298.
40 M. N. Vu, H. G. Kelly, H. X. Tan, J. A. J, R. E, T. P. Davis, N. P. Truong, A. K. Wheatley and S. J. Kent, Hemagglutinin Functionalized Liposomal Vaccines Enhance Germinal Center and Follicular Helper T Cell Immunity, *Adv. Healthcare Mater.*, 2021, **10**, 2002142.
41 J. A. Kulkarni, M. M. Darjuan, J. E. Mercer, S. Chen, R. van der Meel, J. L. Thewalt, Y. Y. C. Tam and P. R. Cullis, On the Formation and Morphology of Lipid Nanoparticles Containing Ionizable Cationic Lipids and siRNA, *ACS Nano*, 2018, **12**, 4787–4795.
42 N. Hussain, B. Singh, T. Sakthivel and A. T. Florence, Formulation and stability of surface-tethered DNA-gold-dendron nanoparticles, *Int. J. Pharm.*, 2003, **254**, 27–31.
43 S. Moffatt and R. J. Cristiano, Uptake characteristics of NGR-coupled stealth PEI/pDNA nanoparticles loaded with PLGA-PEG-PLGA tri-block copolymer for targeted delivery to human monocyte-derived dendritic cells, *Int. J. Pharm.*, 2006, **321**, 143–154.
44 C. Olbrich, U. Bakowsky, C. M. Lehr, R. H. Muller and C. Kneuer, Cationic solid-lipid nanoparticles can efficiently bind and transfect plasmid DNA, *J. Controlled Release*, 2001, **77**, 345–355.
45 R. Whitfield, A. Anastasaki, N. P. Truong, A. B. Cook, M. Omedes-Pujol, V. L. Rose, T. A. H. Nguyen, J. A. Burns, S. Perrier, T. P. Davis and D. M. Haddleton, Efficient Binding, Protection, and Self-Release of dsRNA in Soil by Linear and Star Cationic Polymers, *ACS Macro Lett.*, 2018, **7**, 909–915.
46 P. E. Saw, X. Xu, M. Zhang, S. Cao, O. C. Farokhzad and J. Wu, Nanostructure Engineering by Simple Tuning of Lipid Combinations, *Angew. Chem., Int. Ed.*, 2020, **59**, 6249–6252.
47 Y. K. Huang, H. M. Liu, W. Chen, M. P. Nieh and Y. Lei, Genetically engineered bio-nanoparticles with co-expressed enzyme reporter and recognition element for IgG immunoassay, *Sens. Actuators, Rep.*, 2019, **1**, 100003.
48 R. Tiwari and K. Pathak, Nanostructured lipid carrier versus solid lipid nanoparticles of simvastatin: Comparative analysis of characteristics, pharmacokinetics and tissue uptake, *Int. J. Pharm.*, 2011, **415**, 232–243.
49 J. A. Kulkarni, J. L. Myhre, S. Chen, Y. Y. C. Tam, A. Danescu, J. M. Richman and P. R. Cullis, Design of lipid nanoparticles for in vitro and in vivo delivery of plasmid DNA, *Nanomedicine*, 2017, **13**, 1377–1387.
50 T. Suzuki, Y. Suzuki, T. Hihara, K. Kubara, K. Kondo, K. Hyodo, K. Yamazaki, T. Ishida and H. Ishihara, PEG shedding-rate-dependent blood clearance of PEGylated lipid nanoparticles in mice: Faster PEG shedding attenuates anti-PEG IgM production, *Int. J. Pharm.*, 2020, **588**, 119792.
51 S. Chen, Y. Y. C. Tam, P. J. C. Lin, A. K. K. Leung, Y. K. Tam and P. R. Cullis, Development of lipid nanoparticle formulations of siRNA for hepatocyte gene silencing following subcutaneous administration, *J. Controlled Release*, 2014, **196**, 106–112.
52 K. Shiraishi, M. Hamano, H. L. Ma, K. Kawano, Y. Maitani, T. Aoshi, K. J. Ishii and M. Yokoyama, Hydrophobic blocks of PEG-conjugates play a significant role in the accelerated blood clearance (ABC) phenomenon, *J. Controlled Release*, 2013, **165**, 183–190.
53 O. S. Fenton, K. J. Kauffman, J. C. Kaczmarek, R. L. McClellan, S. Jhunjhunwala, M. W. Tibbitt, M. H. D. Zeng, E. A. Appel, J. R. Dorkin, F. F. Mir, J. H. Yang, M. A. Oberli, M. W. Heartlein, F. DeRosa, R. Langer and D. G. Anderson, Synthesis and Biological Evaluation of Ionizable Lipid Materials for the In Vivo Delivery of Messenger RNA to B Lymphocytes, *Adv. Mater.*, 2017, **29**, 1606944.
54 S. Kimura, I. A. Khalil, Y. H. A. Elewa and H. Harashima, Novel lipid combination for delivery of plasmid DNA to

immune cells in the spleen, *J. Controlled Release*, 2021, **330**, 753–764.
55 Y. Wan, P. M. Moyle and I. Toth, Endosome Escape Strategies for Improving the Efficacy of Oligonucleotide Delivery Systems, *Curr. Med. Chem.*, 2015, **22**, 3326–3346.
56 Y. Suzuki and H. Ishihara, Structure, activity and uptake mechanism of siRNA-lipid nanoparticles with an asymmetric ionizable lipid, *Int. J. Pharm.*, 2016, **510**, 350–358.
57 J. Heyes, L. Palmer, K. Bremner and I. MacLachlan, Cationic lipid saturation influences intracellular delivery of encapsulated nucleic acids, *J. Controlled Release*, 2005, **107**, 276–287.
58 Y. C. Tseng, S. Mozumdar and L. Huang, Lipid-based systemic delivery of siRNA, *Adv. Drug Delivery Rev.*, 2009, **61**, 721–731.